pH-responsive, thermoset polymer coatings for active protection against aluminum corrosion

Joseph Watson[a], Victoria Balmforth[b], Elaine Gray[b] and Matthew G. Unthank[*a]

AUTHOR ADDRESS

a: Northumbria University, Newcastle upon Tyne NE1 8ST, UK. matthew.unthank@northumbria.ac.uk

b: AkzoNobel, Polymer Development Group, Stoneygate Lane, Felling, Tyne & Wear, NE10 0JY, UK.

*: Department of Applied Science, Northumbria University, Newcastle upon Tyne NE1 8ST, UK. matthew.unthank@northumbria.ac.uk

KEYWORDS: Coating, Polymers, Polymer Coatings, Material Interfaces, Corrosion Protection, Filiform Corrosion, Responsive polymers.

ABSTRACT: This paper describes the synthesis and use of multi-functional methacrylic monomers, that contain basic (amine) functional groups, including an example in which an acid labile *tert*-butylcarbamate protected glycine is used to form a novel methacrylic monomer. The 'protected' amino-acid derived functional monomer (BOC-Gly-MA) is co-polymerized with an epoxide functional methacrylic monomer (GMA), to deliver novel multi-functional polymers which are processed into powder coatings and used to study filiform corrosion at the surface of an aluminum substrate. The BOC-Gly-MA containing co-polymers were shown to improve a coating's anti-corrosion performance, presenting the lowest average filiform corrosion (FFC) track length, total FFC number, and total corroded surface area (CSA) of the coatings investigated. Further to this, a mode-of-action for the role of BOC-Gly functional polymers in corrosion protection is proposed, supported by both solution and polymer-aluminum interface studies, delivering new insight into the mode-of-action of pH-responsive polymer coatings.

INTRODUCTION

Organic polymer coatings provide corrosion protection to metal substrates and are widely used across a range of industries, from architectural, marine, and automotive.[1,2] Powder coatings are extensively used in the automotive industry, due to their ability to effectively and efficiently coat metallic substrates via electrostatic application methods. In this process, charged powder coating particles (consisting of polymers, crosslinkers and additives) are attracted to the electrically earthed substrate, producing a thin uniform coating across the entirety of the metal surface.[3–5] High optical clarity powder coatings for high aesthetic demand applications, such as the protection of aluminum-alloy wheels, are typically based on epoxide functional acrylic co-polymers, crosslinked with flexible C8-C12 diacids such as sebacic or dodecanoic acid. Such coatings deliver a combination of excellent mechanical properties, chemical resistance, and optical clarity.[3,6–10] Polymer coatings act as a physical barrier protecting the metal surface from corrosion; however this passive protection is only effective as long as the coating remains intact and the entire wheel (including edges) are coated with a protective layer of polymer.[11–13]

A major performance challenge of polymer coated aluminum is the materials susceptibility to filiform corrosion (FFC).[14] FFC initiates at areas of coating damage, defect or low film thickness, which allows corrosive media (particularly aqueous chlorides and acids) to reach the metal surface.[15] Water, oxygen and ions permeate the coating and the FFC tail, fueling the redox process at the filiform head, thus causing FFC propagation under the coating, increasing the degree of damage and loss of attractive aesthetic appearance.[16] Coatings designed solely for barrier protection, only remain effective in corrosion prevention, when undamaged and adhered to a metallic surface. Due to this limitation, chemical 'active corrosion protection' additives are often dispersed within the organic coatings to improve their protective abilities.[17] The main routes to achieving active corrosion protection are through incorporation of reactive species into the coatings such as inorganic fillers for instance $CeCl_3$, Li_2CO_3 or MoO_2^{-4} (and historically chromates),[17] or alternatively through dispersion of low solubility organic compounds including 2-mercaptobenzothiazole, imidazole derivatives or benzotriazoles, dispersed either within the coating, or contained within micro-capsules.[18–21]

Previous research has measured the pH of the filiform head, to be within the range of pH 1.0-2.5,[22,23] caused by high concentrations of Al^{3+} ions in solution. As the aqueous acidic conditions within a filiform corrosion cell are well described, polymers (and subsequent polymeric coatings) could potentially be designed to act upon these environmental triggers. Research has studied the use of semi-soluble lithium salts (Li_2CO_3, and $Li_2C_2O_4$) which can inhibit corrosion through increasing pH and promoting the formation of a protective layer at the damaged coating area.[24–32] Upon coating damage and exposure to a corrosive environment, lithium salts were reported to leach from the coating, to the site of coating damage where it was able to form a passivating layer, protecting the coating surface from further corrosion propagation. However, the dispersion of lithium salts in the otherwise transparent organic coatings, resulted in an opaque finish, and as such this approach is not viable for high optical clarity powder coatings, such as those required for the protection of aluminum-alloy wheels.

In the research described here, we propose that the inclusion of selected chemical functionalities within the polymer backbone itself may be a route to minimization of FFC (through

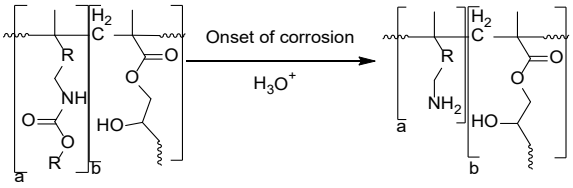

Figure 1: Proposed mode of action for pH activated protecting group removal, post polymerisation.

increasing pH), whilst also maintaining optical clarity. It was hypothesized that a polymer tethered with amine functionalities may be suitable for this process, as they would buffer the low (acidic) pH at the propagating filiform head, increasing pH. However, the inclusion of amine functionality in epoxy-based thermosetting polymer coatings for aluminum protection, presents significant technical challenges. Amines are well known to be a) highly reactive nucleophiles that undergo (often multiple) addition reactions with epoxide groups, also used in thermosetting powder coatings[33, 34] and b) prone to discoloration in coatings (via *N*-oxidation).[35] One solution to this issue would be through the use of amine-protecting groups, where deprotection (and concomitant liberation of the basic amine group) occurs under the conditions of filiform corrosion (i.e. pH ~1.0-2.5). The *tert*-butylcarbamate (BOC) protecting group is widely used in the fine chemical and pharmaceutical industries as an acid labile protecting group for amines,[36–41] but to our knowledge has never been studied in coatings for pH responsive corrosion prevention (Figure 1). The use of this functional group may open opportunities to create multifunctional, pH responsive polymers capable for both forming thermoset coatings and preventing propagation of FFC on aluminum substrates.

EXPERIMENTAL

Materials

All materials were purchased from commercial vendors listed in the supplementary information and used as received. The commercial control polymer (COM) was supplied from industrial sponsor AkzoNobel and used as received.

Nuclear Magnetic Resonance (NMR)

NMR analyses were acquired at 25 °C using a JEOL ECS400 Delta spectrometer at frequencies of 399.78 MHz for ^{1}H-NMR, 100.53 MHz for ^{13}C-NMR. All chemical shifts are quoted as parts per million (ppm) relative to tetramethylsilane (TMS, δ=0 ppm) as an internal standard in either deuterated chloroform ($CDCl_3$) or deuterated dimethyl sulfoxide (DMSO-d_6). ^{13}C-NMR assignment was confirmed by DEPT analysis. The spectral data is recorded as chemical shift (δ), relative integral, multiplicity (s=singlet, br=broad, d=doublet, t=triplet, q=quartet, quin=quintet, sext=sextet, dd=doublet of doublets, m=multiplet) and coupling constant (J = Hz).

Fourier Transformed Infrared spectroscopy (FTIR)

Infrared spectroscopy was performed on a Bruker alpha platinum-ATR or a PerkinElmer Spotlight 150i FT-IR microscope, with an aperture of 100 x 100 µm, and the output data analyzed in OPUS or Spectrum 10 software respectively. Absorption maxima are expressed in wavenumbers (cm^{-1}).

Gel Permeation Chromatography (GPC)

Samples were dissolved in THF (2 mg/mL) and filtered through 0.2 µm nylon filters. Samples were analyzed using an Agilent 1260 infinity II system equipped with a refractive index and viscometry detector, fitted with PLgel MiniMIX-E and PLgel MiniMIX-D columns in sequence, using a THF mobile phase and a flow rate of 0.6 mL/min. Analysis was performed against a calibration curve of polystyrene standards (EasiVial PS-M supplied by Agilent).

Thermogravimetric Analysis (TGA)

TGA analysis was conducted using a Perkin-Elmer Pyris 6 TGA thermal analyzer and results interpreted in Pyris software (version 11.1.1.0492). Polymer samples of between 16-20 mg weight were heated in ceramic crucibles from 30 °C to 650 °C at a constant rate of 20 °C per minute, under a flow of N_2 (40 mL/min). The residual mass was recorded as a percentage weight, of the original mass, that remained at 600 °C (within the range where mass remained constant after the degradation of organic material).

Tensile Testing

Thin free film polymer samples for mechanical testing were laser cut to 90 mm x 10 mm using a Glowforge™ Basic laser cutter equipped with a 40 W CO_2 laser tube. Tensile experiments were conducted on either an Instron 5969 or Instron 3343 with a displacement ramp rate of 10 mm per minute using a 1 kN load cell and samples were held in place with mechanical wedge grips.

Synthesis of BOC-Gly-MA.

To a solution of *N*-(*tert*-butoxycarbonyl)glycine (BOC-Gly, 14.730 g, 84.0 mmol) and K_2CO_3 (0.967 g, 7.0 mmol) in THF (20 mL, degassed using N_2) was added glycidyl methacrylate (GMA, 9.950 g, 70.0 mmol) before heating to 50 °C under stirring and N_2. After 24 hours the reaction mixture was cooled to room temperature and diluted with ethyl acetate (100 mL). The reaction mixture was washed with a saturated $NaHCO_3$ solution (3 x 100 mL), the organic phase was collected, and dried over $MgSO_4$. The organic phase was then concentrated under reduced pressure, affording the product as a clear oil as a mixture of isomers (19.98 g, 75%) (85% major 15% minor, by ^{1}H-NMR and LCMS). The product was a mixture of BOC-Gly-MA and unreacted GMA, and the monomer mixture was determined by ^{1}H-NMR and used directly in a radical polymerisation reaction of multifunctional polymers. A small sample was purified by column chromatography for analytical purposes/ δH (400 MHz; $CDCl_3$): 6.13 (s, 1H), 5.61 (s, 1H), 5.03 (s, 1H), 4.31-4.19 (m, 4H), 4.17-4.12 (m, 1H), 3.93 (d, J = 5.5 Hz, 2H), 2.73 (s, 1H), 1.94 (s, 3H), 1.44 (s, 9H). δC (400 MHz; $CDCl_3$): 170.5 (C=O), 167.4 (C=O), 156.2 (C=O), 135.8 (C=C), 126.5 (C=C), 80.3 (C(CH3)), 67.8 (C-O), 66.0 (C-O), 65.1 (C-O), 42.4 ((C=O)CNHR), 28.3 ($C(CH_3)$), 18.3 (CH_3). νmax/cm^{-1} = 3380w (broad), 2975w, 1703s, 1520m, 1367w. MS: (+ESI) ([M+H]) major = m/z 318.155, minor = m/z 318.15.

Table 1: Monomer and initiator compositions for the synthesis of functional polymers.

		Weight%						
Entry	Sample	MMA	GMA	STY	^{i}BOMA	BOC-Gly-MA	DPA-MA	Initiator (mol%)
1	CTL-HT	52	28	4	16	0	0	4T
2	CTL-LT	52	28	4	16	0	0	8A
3	5-BOC-HT	47	28	4	16	5	0	4T
4	5-BOC-LT	47	28	4	16	5	0	8A
5	50-BOC-HT	0	28	0	22	50	0	4T
6	CTL-HT*	52	28	4	16	0	0	4T
7	5-BOC-HT*	47	28	4	16	5	0	4T
8	5-BOC-LT*	47	28	4	16	5	0	8A
9	5-DPA-HT*	47	28	4	16	0	5	4T

* Indicates polymers synthesized at a 1 kilo scale; T and A indicate whether Trigonox 21S (T) or AIBN (A) was used as the radical initiator. MMA (methylmethacrylate), GMA (glycidylmethacrylate), STY (styrene), iBOMA (*iso*-bornylmethacrylate), BOC-Gly-MA (reaction product of *N-(tert*-butoxycarbonyl)glycine and GMA), DPA (*diiso*-propylethylamino-methacrylate). The mass of butyl acetate present in the monomer/initiator mixture was equal to 20% of the total monomer mass. The mass of solvent initially present in the reaction vessel prior to infusion was equal to 50% of the total monomer mass**.**

General method of small-scale polymer synthesis:

A solution of mixed monomers (based on Table 1) and *tert*-butyl peroxy-2-ethylhexanoate (Trigonox 21S) (high-temperature, HT method) or azobisisobutyronitrile (AIBN) (low-temperature, LT method) was prepared and diluted with butyl acetate (HT) or isopropyl acetate (LT) (solvent mass equal to 20% of the total monomer mass). The monomer/initiator mixture was then added to a 100 mL, 3 neck round bottom flask containing butyl acetate (HT) or isopropyl acetate (LT) at a volume equal to 50% of the total monomer mass, pre-heated to 125 °C (HT) or 85 °C (LT). The monomer/initiator mixture was added by use of a syringe pump at a rate of 0.5 mL/min, whilst under N_2 and constant stirring provided by a magnetic stirrer. Once the monomer/initiator mixture addition was complete, the reaction mixture was stirred for a further 1 hour at 125-130 °C (HT) or 85-90 °C (LT). The polymer-solvent mixture was then poured into aluminum foil lined trays and placed into a vacuum oven (-1020 mbar) at 100 °C (HT) or 85 °C (LT) for 3 hours to remove solvent and non-polymerized monomer.

General method of large-scale polymer synthesis:

A solution of mixed monomers (based on Table 1) and Trigonox 21S (HT) or AIBN (LT) was prepared and diluted with butyl acetate (HT and LT) (solvent mass equal to 20% of the total monomer mass). The monomer/initiator mixture was then added to a pre-heated 2 L flange neck flask containing butyl acetate (at a volume equal to 50% of the monomer mass), and pre-heated to 125 °C (HT) or 85 °C (LT). The monomer/initiator mixture was added via use of a peristaltic pump at a rate of 7.4 mL/min over 3 hours, whilst under N_2 and constant stirring provided by an overhead stirrer. Once the monomer/initiator mixture addition was complete, the reaction mixture was stirred for a further 1 hour at 125-130 °C (HT) or 85-90 °C (LT). A solution of Trigonox 21S (HT) or AIBN (LT) equal to 10% mass of initial initiator weight was then added to the reaction as a single charge, whilst stirring at a temperature of 125-130 °C (HT) or 85-90 °C (LT) was maintained for a further 45 minutes. The reaction was then maintained at 100 °C and a distillation was performed to remove most of the reaction solvent. After 40 minutes of distillation under vacuum, the polymer mixture was poured into foil lined trays, and placed into a vacuum oven (-1020 mbar) at 100 °C (HT) or 85 °C (LT) for 3 hours to remove residual solvent and non-polymerized monomer. The co-monomer and initiator formulations for all polymers synthesized throughout this research are detailed in Table 1.

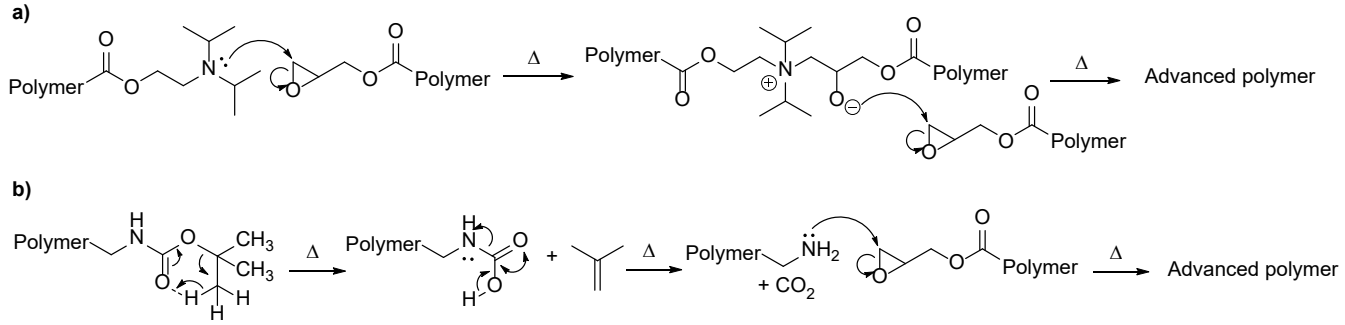

Scheme 1: a) The proposed mechanism for advancement of co-polymers of DPA-MA and GMA and b) The proposed mechanism for advancement of co-polymers of BOC-Gly-MA and GMA.

RESULTS AND DISCUSSION

To study the concept of incorporating amine functionality in epoxide based acrylic powder coatings, two monomers were selected for this investigation (Figure 2). 2-(Diisopropylamino)ethyl methacrylate (DPA-MA) was selected as a basic amine functional monomer, whereby the significant steric hinderance offered by *N*-diisopropyl functionality was chosen to suppress nucleophilic addition to epoxide groups, perhaps allowing co-polymerisation under radical initiated conditions. To study alongside DPA-MA, we synthesized a *tert*-butylcarbamate (BOC) functional methacrylic monomer, from readily available starting materials. We selected the amino acid glycine for this purpose as the BOC protected amine functional building block.[42] BOC protected amino acids are commonly used in polypeptide synthesis in the biopharmaceutical industry and as such BOC-amino acids are commercially available.[43–45] We looked to exploit the widely known carboxylic acid-epoxide ring opening reaction to allow the reaction of *N*-*tert*-butylcarbamate glycine (BOC-Gly) and glycidyl methacrylate (GMA, Figure 2), to synthesize a new monomer (BOC-Gly-MA) containing both methacrylate functionality (for radical polymerisation) and BOC functionality (to study deprotection under filiform corrosion conditions).

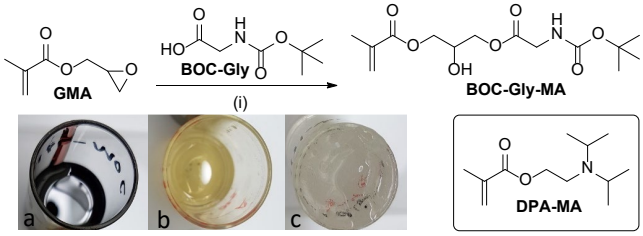

Figure 2: Synthesis of BOC-GLY-MA and structure of DPA-MA. (i) K_2CO_3, THF. Images a to c represent the degree of discoloration from original reaction conditions (a, dark colored) to purification using activated carbon filtration (b, pale yellow) and finally optimization of reaction condition to eliminate color (c, clear).

BOC-Gly-MA was synthesized using base catalyzed ring opening of GMA (Figure 2). Conducting this reaction at 80 °C, resulted in significant discoloration during the synthesis (Figure 2, image a). As BOC-Gly-MA was intended for co-polymerisation and applications in high clarity, transparent powder coatings, discoloration could not be tolerated. Initial attempts to remove the color through activated carbon filtration[46] was only partially successful (Figure 2, image b), so an investigation was conducted to identify the source of color formation. Chromatographic separation of the reaction components revealed that mixed aromatic derivatives (of *tert*-butyl hydroquinone) were the likely cause of the discoloration, formed at the elevated reaction temperature (80 °C).[47–49] It was found that by reducing the reaction temperature to 50 °C and increasing the mole percentage of K_2CO_3 from 5 to 10% the reaction could deliver a 75% yield of BOC-Gly-MA on a multigram scale, as a clear and colorless product (Figure 2, image c). Optimal conditions for the synthesis found that separation of any unreacted GMA from the BOC-Gly-MA product was not necessary since GMA was an ingredient in all of the functional polymer synthesized (all at 28% w/w GMA). The resulting BOC-Gly-MA/GMA mixture was thus used directly in the polymerisation reactions, and the additional GMA was conveniently added to achieve the target concentration of 28% w/w. The BOC-Gly-MA functional monomer was co-polymerized with methyl methacrylate (MMA), glycidyl methacrylate (GMA), *iso*-bornyl methacrylate (iBOMA) and styrene (STY) at 125 °C (HT conditions). MMA was selected due to the high clarity polymers it can produce combined with a relative low monomer cost. GMA provides the polymer with reactive functional groups capable of forming a thermoset (network) polymer on reaction with an aliphatic diacid (sebacic acid). iBOMA is used to increase the T_g of the final polymer (and resulting) coating so that it would remain in the glassy state at the desired operating temperature. Finally, a low level of styrene (4 wt%) is included to improve final mechanical properties of the coating.[50]

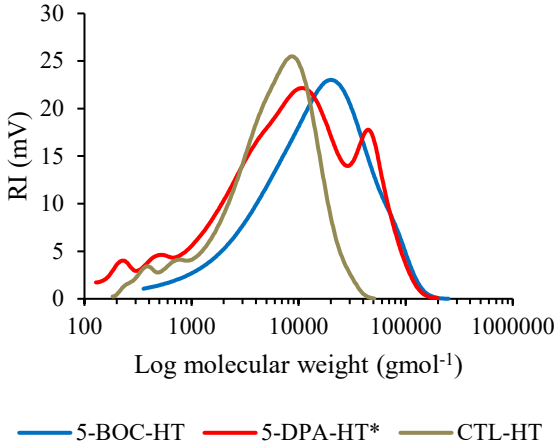

Figure 3: GPC chromatogram of control, 5-DPA-HT* and 5-BOC-HT, numbered labels represent the PD of the peak.

The polymerisation product (Table 2, Entry 3, 5-BOC-HT) was studied by GPC (Figure 3) which showed a significantly increased Mn and Mw, partnered with a significant increase in polydispersity (PD) illustrated by peak broadening when compared to the control polymer (Table 2, Entry 1, CTL-HT) which did not contain BOC-Gly-MA. This result can be attributed to the presence of the BOC-Gly-MA in the co-polymerisation with GMA, promoting polymer-to-polymer bond forming reactions (known as advancement), causing the observed increase in M_w and resulting polydispersity (Table 2, Entry 1 vs 3). Polymer-to-polymer bond forming reactions increase both polydispersity and average functionality (i.e. the average number of reactive functional groups per polymer chain) of the resulting polymer chains. An increase in functionality results in a reduction in the critical extent of reaction required for gelation (p_{gel}, as described by Flory and Stockmayer)[51,52] which in-turn impacts flow and coalescence in powder coatings. Poor coalescence in powder coatings negatively impacts both aesthetic appearance and mechanical properties.[53] The polymerisation of hindered tertiary amine monomer DPA-MA, resulted in a further increase of polymer-to-polymer bond formation, as characterised by a very high polydispersity of 7.95 and emergence of a second, higher molecular weight peak in the GPC chromatogram, characteristic of advancement (Figure 3). The high polydispersity of the co-polymer containing 5% w/w DPA-MA monomer (Table 2, Entry 8) is attributed to the failure of the diisopropyl functionality to provide sufficient steric hinderance to prevent reaction with the co-existing epoxide groups (from GMA monomer) at high polymerisation temperatures of 125 °C. The tertiary amine of the diisopropylamine functional groups participate in

nucleophilic ring opening with the co-existing epoxide groups on adjacent polymer chains, resulting in polymer-to-polymer bond formation (i.e., advancement, as illustrated in Scheme 1). Tertiary amines are known to promote anionic polymerisation via this mechanism, leading to further epoxide ring opening reactions, resulting in the formation of a high polydispersity polymeric mixture.[54,55] *tert*-Butylcarbamate groups (BOC) are not typically regarded as nucleophilic, so it was proposed that some of the BOC protecting group must be removed during the high temperature conditions of polymerisation liberating a primary amine, which would then undergo facile reaction with the epoxide groups also present in the formulation,[56,57] resulting in polymer-to-polymer bond formation and increased polydispersity (Scheme 1). To study the proposed thermally initiated BOC removal, a series of model studies were designed to understand the effect of temperature on BOC deprotection.

As the removal of the BOC group produces CO_2 and isobutene, (both of which are volatile gasses), thermogravimetric analysis (TGA) was used to study the effects of temperature on BOC group retention/removal. A series of experiments were conducted using BOC protected glycine (BOC-Gly) as a (non-polymerizable) model for the BOC-Gly-MA. To mimic the conditions of thermally initiated radical polymerisation, BOC-Gly was held at either 130 °C or 90 °C for 3 hours in a TGA and the mass loss recorded over time. The results of the TGA experiment presented in Figure 4 show a 47% reduction in mass of BOC-Gly at 130 °C, over the 3-hour duration of the experiment. When exposed to lower temperature conditions of 90 °C for 3 hours there was no detectable loss of mass, indicating that BOC functional group are stable under these conditions. Glycine was also tested as a control where it was exposed to 130 °C for 3 hours and did not show any mass loss, confirming the mass loss was related to the presence of the *tert*-butylcarbamate group.

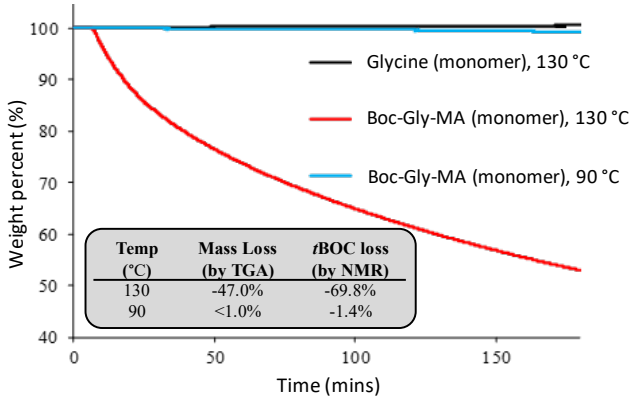

Figure 4: Mass loss study using TGA and (insert) calculated final mass loss (TGA) and estimated *tert*-butylcarbamate (BOC) loss by ^{1}H-NMR. HT = 130 °C and LT = 90 °C.

^{1}H-NMR was also used to analyze the reaction product after the TGA experiments (Figure 4, inset). Integration of *tert*-butyl ($(CH_3)_3$) against H_2NCH_2- allowed an estimation of the degree of BOC protection group removal when heated (see supp. data for details). Comparison of the BOC-Gly-HT (130 °C) reaction product with glycine control confirmed the presence of glycine (Gly) in the reaction product, formed via thermal deprotection of the BOC group. The BOC-Gly-LT (90 °C) reaction in contrast showed no sign of glycine formation, supporting the hypothesis that the BOC functional group remained intact at this lower temperature.

Table 2: A summary of GPC and DSC analysis of the range of polymers synthesized in this study. * Denotes kilo scale synthesis. All others are 5g scale synthesis.

Entry	Sample	Mn	Mw	PD	T_g (°C)
1	CTL-HT	2730	8596	3.15	66.1
2	CTL-LT	3190	7615	2.39	58.8
3	5-BOC-HT	6062	23383	3.86	67.0
4	5-BOC-LT	3033	7513	2.48	54.0
5	CTL-HT*	2654	7647	2.88	67.7
6	5-BOC-HT*	2591	8717	3.36	57.5
7	5-BOC-LT*	3065	5387	1.76	53.8
8	5-DPA-HT*	2281	18138	7.95	55.1

These results suggest that a reduction in polymerisation temperature to 90 °C, should allow co-polymerisation of BOC-Gly-MA and GMA, whilst minimizing BOC deprotection and associated polymer-to-polymer bond formation (as depicted in Scheme 1b). Polymer, 5-BOC-LT was therefore synthesized using 5wt% BOC-Gly-MA and 28wt% GMA (Table 1, Entry 4) at 90 °C. ^{1}H-NMR analysis (supplementary information, Table S9) showed that polymer 5-BOC-LT, suffered minimal (<8%) loss of BOC group, which compared favorably to 5-BOC-HT (Table 1, Entry 3) which suffered 28% loss of BOC. This loss of BOC functionality directly effects the polydispersity of the functional polymer as shown in Table 2. Polymer 5-BOC-HT (Table 2, Entry 3) showed a polydispersity of 3.86, which decreased to 2.48 (Table 2, Entry 4, 5-BOC-LT) at the lower temperature of polymerisation. The 5-BOC-LT (Table 2, Entry 4) also compares favorably with the control polymers containing 28%wt GMA only (0% BOC-Gly-MA) which showed a very similar polydispersity of 2.39 under low temperature (LT, 90 °C) conditions (Table 2, Entry 2, CTL-LT). This result shows that at 90 °C there is no significant impact on polydispersity of using BOC-Gly-MA in a co-polymerisation with GMA.

A reduction in T_g could also be seen when comparing LT to HT control polymers by DSC (-7.3 °C), which is also mirrored in the functional polymers, with a loss of 13 and 3.7 °C in T_g of small- and kilo-scale polymers respectively. This reduction in T_g can be explained by the reduction of polymer advancement (shown by reduction in PD) which can be attributed to a reduced number of chain-to-chain bonds forming reactions, increasing the rotational freedom and resulting free-volume of the polymer chains, thus decreasing the T_g.[58] As functional monomer concentration in the polymer formulation is increased, the concentration of MMA is decreased proportionately, which can also contribute to a reduction in T_g by DSC (polymethylmethacrylate has a relatively high $T_g\infty$). This can be seen when comparing the T_g (by DSC) of the CTL-LT (Table 2, Entry 2) and the non-advanced functional polymers synthesized under LT conditions (Table 2, Entry 4 and 7).[59]

As powder coating manufacture requires significant quantities of polymer for formulation, melt extrusion, milling, sieving, and spraying, 5-BOC-HT, 5-BOC-LT, 5-DPA-HT, and CTL-LT were manufactured on a 1kg (final weight) scale (denoted by * in Entries 5-8, Table 2). Using slow monomer addition

(starved feed) to control internal reaction temperature, the 5-BOC-LT* polymer was synthesized on a 1 kg scale, delivering the lowest polydispersity product so far (PD = 1.76, Table 2, Entry 7), which compared very favorably to the 5-BOC-HT* polymer, with a high polydispersity of 3.36 (Table 2, Entry 6). The 1 kg synthesis of 5-DPA-HT* was manufactured for comparison, resulting in the highest polydispersity product (PD = 7.95, Table 2, Entry 8), as a result of epoxy ring opening promoted by diisopropyl functional groups (as depicted in Scheme 1a). To study the effect of BOC-Gly-MA and DPA-MA functional polymers on filiform corrosion performance, the CTL-HT*, 5-BOC-HT*, 5-BOC-LT*, and 5-DPA-HT* (Table 2, Entries 5-8) polymers were formulated into powder coatings, which were subsequently sprayed onto cast aluminum panels (A356 alloy, in-line with aluminum alloy wheels), mechanically scribed, and subjected to accelerated filiform corrosion testing according to procedure SAE J2635 (see supp. data for details). Analysis of corrosion was conducted using a Quantiz analytical system to measure filiform corrosion (FFC) track length, FFC track number, FFC width, and total corroded surface area (CSA).

The results in Figure 5 (FFC length, orange sphere) show that a powder coating manufactured from 5-BOC-LT* had the lowest average FFC track length (0.748 mm, Figure 5, Entry 3), with a combination of Kruskal-Wallis and Dunn's post-hoc testing proposing that a coating which contained 5% w/w BOC-MA functional monomer and synthesized using LT polymerization conditions (5-BOC-LT*) is more likely to display a significantly shorter average FFC track length than coatings synthesized using HT polymerization conditions, or containing an alternate functional monomer (i.e. 5-BOC-HT*, 5-DPA-HT*) (see supplementary data for details). When comparing the results of average FFC number (count) per panel (FFC count, blue bar, Figure 5), coatings based on 5-BOC-LT* was shown again to improve anti-corrosion performance compared to 5-BOC-HT*, Control-HT (CTL-HT) and even a standard commercial acrylic coating (COM, see Figure 5, Entry 3 vs Entries 4, 1 and 2 respectively). Finally, when comparing the coatings average corroded surface area (CSA, green bar, Figure 5) it can be seen there is a substantial difference in corrosion performance from the powder coating based on 5-BOC-LT* (Figure 5, Entry 3, CSA = 52.7 mm^2) in comparison with those based on 5-BOC-HT* (Figure 5, Entry 4, CSA = 127.3 mm^2) and 5-DPA-HT* (Figure 5, Entry 5, CSA = 90.5 mm^2).

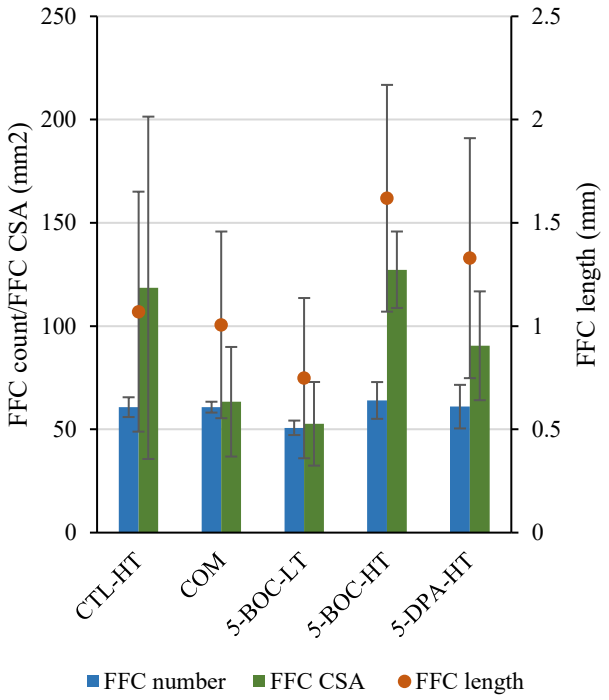

Figure 5: Results of FFC length, FFC count (number) and average CSA from powder coated aluminum subjected to corrosion testing. Standard deviation was used to calculate the error for FFC number and CSA as the data was normally distributed, while MAD was used to calculate the error for the non-normally distributed FFC length.

The corrosion results show that in the powder coatings where the parent polymers have identical monomer composition (and accompanying 'reactive' functionality, Table 1, Entries 7 and 8, 5-BOC-LT* vs 5-BOC-HT*) advancement, induced by *in-situ* deprotection of *tert*-butylcarbamate groups (BOC), has a substantial and detrimental impact on corrosion performance, across the three key metrics used in this study (i.e. average FFC track length, total FFC number (count) and average corroded surface area, Figure 5, Entry 3 vs. 4). The results provide evidence of the importance of optimizing the polymerisation reaction conditions, to minimize polydispersity induced by advancement. This is particularly important when using multiple 'reactive' or functional monomers, particularly when potential polymer-to-polymer bond forming reactions are possible. While it was clear that coatings based on advanced polymers performed less well in corrosion testing than equivalent less-advanced coatings, the root-cause of this difference required further investigation. A study of coating material properties was conducted to further understand this effect.

Powder coatings were prepared as non-adhered 'free' films based on polymers CTL-HT*, 5-BOC-HT*, 5-BOC-LT* and 5-DPA-HT* (see experimental section 1.2 - Powder Coating Manufacture for details). All coating systems were studied using tensile testing and the results are illustrated in Figure 6, highlighting Young's modulus (YM, MPa) and ultimate tensile strength (UTS, MPa)). The results showed that coatings based on polymers 5-BOC-HT* and 5-BOC-LT* measured Young's moduli of 2524 and 2351 MPa respectively, which were both similar to the CTL-HT* control coating which lacked the presence of the BOC-Gly-MA monomer (YM = 2578 MPa).

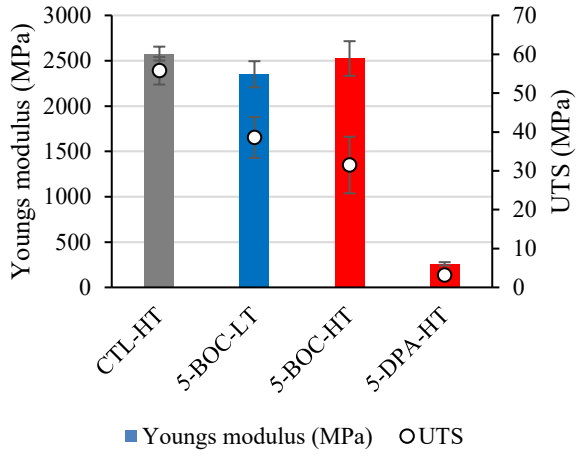

Figure 6: The Youngs modules (YM) and ultimate tensile strength (UTS) results for the four powder coatings based on the large-scale (1 kg) polymerisation products.

Coatings based on the most advanced polymer 5-DPA-HT displayed significantly lower ultimate tensile strength values (UTS = 3.16 MPa), when compared to the CTL-HT* control coating (UTS = 55.8 MPa) or the coatings containing the BOC-Gly-MA monomer (5-BOC-LT* UTS = 38.6 and 5-BOC-HT* UTS = 31.5). Generally, coatings based on highly advanced polymer 5-DPA-HT* showed very poor mechanical performance via both metrics, with a Young's modulus of 259.5 MPa and UTS of 3.16 MPa. This can be attributed to advancement during the polymerisation stage, which results in embrittlement of the resulting coating, contributing to poor corrosion performance. The coating metrics found to have the greatest correlation coefficient and R^2 were the Young's modulus and average FFC width (0.9848, 0.9699, Figure 7) and the Young's modulus (MPa) and total corroded surface area (mm^2) (0.9488, 0.9003, Figure 8). The results displayed in Figure 7 and Figure 8 support the hypothesis that high Young's modulus coatings may be more susceptible to filiform corrosion. Previous research noted the movement of filiform corrosion progresses in a stepwise segmental manner,[60] as such it was theorized that as filiform corrosion moved across the aluminum-coating interface, stiffer (high Young's modulus) coatings may experience a greater segmental area of coating disbondment, linked to FFC width and CSA. While more flexible coatings (low Young's modulus) were theorized to yield with increased ease, resulting in reduced segments of coating removal, with each step of FFC propagation.

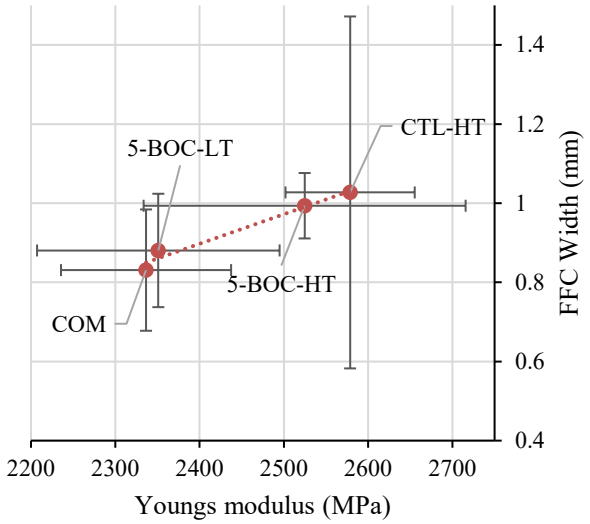

Figure 7: The correlation observed when comparing a coating's Young's modulus to the average FFC width.

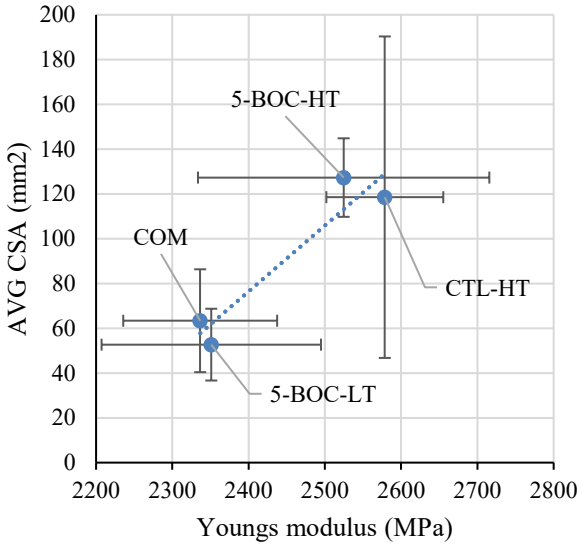

Figure 8: The correlation observed when comparing a coating's Young's modulus to the total corroded surface area (CSA).

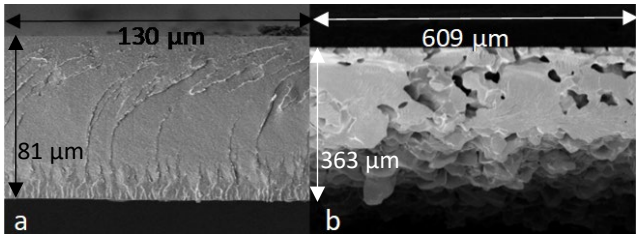

Figure 9: SEM image showing cross-section of coatings based on a) 5-BOC-HT* and b) 5-DPA-HT*. The difference in coating thickness (5-BOC-HT 0.081mm, 5-DPA-HT 0.363) required an increased field of view for 5-DPA-HT

Cross-sectional analysis of coatings based on polymers 5-BOC-HT* (polydispersity = 3.36) and 5-DPA-HT* (polydispersity = 7.95) was conducted using SEM (Figure 9). This study exposed a poor degree of powder particle coalescence in coatings made from the highest polydispersity (i.e., most advanced) 5-DPA-HT* polymer. During the powder coating application process, heat is applied to the powder coated substrate, to promote melting, flow, and coalescence of the powder particles into a single cohesive film (i.e., the final coating). Failure of this process (due to poor particle flow and coalescence) can result in a coating with poor cohesive strength, made from 'fused/sintered powder particles' rather than a fully coalesced coating. In the case of coatings based on the 5-DPA-HT* polymer, the very high degree of advancement causes both i) increased melt viscosity of the 5-DPA-HT* polymer in the molten state and ii) an increase in weight average functionality (f_w) of the polymer. High melt viscosity results in poor flow and coalescence in the melt state, contributing to the poor mechanical performance of coatings based on the 5-DPA-HT* polymer. Increased f_w results in a decrease in the critical extent of reaction required for gelation (p_{gel}),[52] thus gelation occurs at a lower extent of reaction, which also limits opportunity for polymer flow and particle coalescence. Both factors contribute to the porous coating structure for the 5-DPA-HT* polymer shown in Figure 9b, and poor mechanical properties represented in (Figure 6, Entry 4).

We have demonstrated the ability to introduce *tert*-butylcarbamate (BOC) protected amine functionality into a multi-functional polymer with GMA whilst causing minimal advancement (Table 2, Entry 7, 5-BOC-LT*). We have also shown that the resulting polymer could be used to form thermoset powder coatings with favorable corrosion performance when compared to the existing commercial powder coatings (Figure 5). The next stage of the research was to determine whether acid-mediated *tert*-butylcarbamate (BOC) deprotection of the functional coating occurred under the low pH environment of a FFC corrosion head, thus supporting pH buffering as the likely mode-of-action for enhanced corrosion protection. To enhance the concentration of BOC functional groups for analysis, whilst maintaining the ability to form a thermoset coating, a multi-functional polymer based on 50wt% BOC-Gly-MA and 28wt% GMA monomer was synthesized (Table 1, Entry 5, 50-BOC-HT) and studied in both solution model tests and coating model tests.

For solution model testing, polymer 50-BOC-HT was exposed to conditions designed to mimic the acidic aqueous environment of the filiform corrosion process. Accordingly, a 4M HCl(aq.)/THF (1:1 v/v) was prepared and samples of 50-BOC-HT polymer were submerged into the solution. At each time point (1-7 days) a sample was removed, dried and changes in

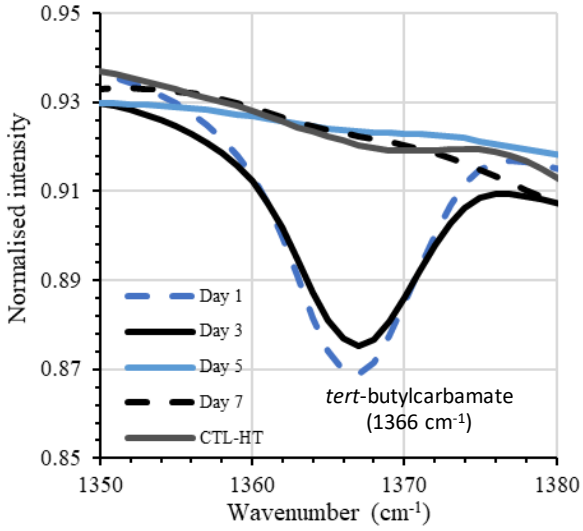

Figure 10: Overlay of IR spectra recorded in transmittance mode between 1350-1380 cm^{-1}, taken over the 7-day model corrosion test period. Focusing on the area which displays the depleting signal produced by the tert-butylcarbamate (BOC) group over time.

the polymer functional groups were studied by infra-red spectroscopy. The relative peak intensity of the *tert*-butylcarbamate (BOC) signal at 1366 cm^{-1} was compared to the (hydrolytically stable) aliphatic polymer backbone -CH_3 and -CH_2- bond signal at 1470-1430 cm^{-1}, to measure the reduction in BOC protecting group concentration over the 7-day period (see supplementary data for details). The results showed that the concentration of BOC protecting group was significantly reduced over the 7-day study period, observed through reduction in peak intensity at 1366 cm^{-1}, when compared to a control experiment under neutral (non-acidic, pH = 7.0) conditions (Figure 10). This result was support by ^{1}H-NMR analysis over the 7 days study, which indicated a 67% reduction in *tert*-butylcarbamate signals (1.44 ppm), relative to polymer backbone -CH_3 groups (3.73 ppm).

Studying the concentration of BOC functionality at the coating-metal interface was more challenging. Accordingly, 50-BOC-HT polymer was formulated and cured into a thermoset coating and applied on a 25 mm x 25 mm aluminum Q-panel (Figure11a, 'aluminum panel'). The coated Q-panel was placed (coated face down) on to an aluminum A356 alloy panel (Figure11a, 'Cast aluminum substrate B'), prepared according to the casting and machining process of an aluminum alloy wheel. The substrates were then clamped together according to the illustration in Figure11a. The resulting test unit was exposed to a corrosion process of 6 hours of copper accelerated-acetic acid salt spray (CASS), before placing in a humidly and temperature-controlled chamber (85% relative humidity at 60 °C) for 28 days to promote filiform corrosion from the exposed edge. The samples were then disassembled (see Figure11b) and the coating surface (previously in contact with 'cast aluminum substrate B') was analyzed using an infra-red spectroscopy microscope. The relative abundance of *tert*-butylcarbamate (1395-1385 cm^{-1}) was collected by infra-red spectroscopy vs a baseline value obtained (in triplicate) prior to exposure to the corrosion testing and presented as a 6 x 6 grid (Figure11c, green illustrates no change within the standard deviation of the baseline samples, yellow to red indicates a percentage reduction in *tert*-butylcarbamate concentration on the coating surface). Analysis

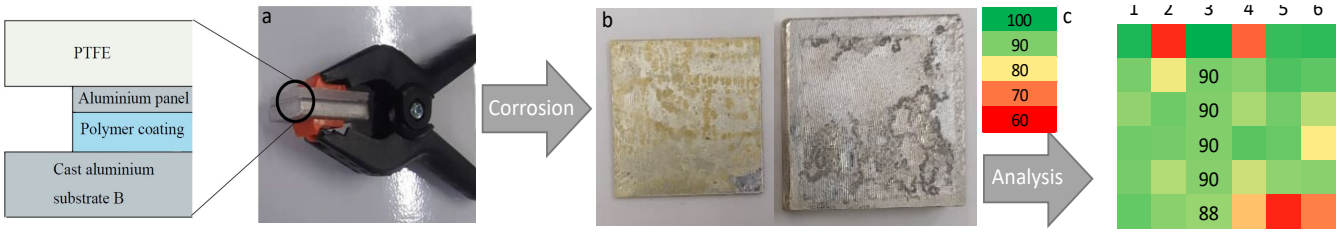

Figure 11: a) Assembled clamped sample of 50-BOC-HT coating prior to subjection of accelerated corrosion conditions; b) disassembled clamped sample after CASS exposure and 30 days in a humidity chamber; c) Grid with values representing the percentage of BOC groups remaining.

indicates that the greatest reduction in *tert*-butylcarbamate concentration (37%) was more often found around the sample edge, in contrast little or no change in *tert*-butylcarbamate concentration was observed in the sample center. The sample edge in this experiment is analogous to an area of coating which has sustained damage, which is the initiation site for the FFC displayed in Figure11b. The aqueous acidic environment caused by the propagating FFC trails were proposed to be the cause for the *tert*-butylcarbamate concentration reduction. These results align with the hypothesis that the aqueous low pH environment created in the presence of filiform corrosion is sufficiently acidic to remove *tert*-butylcarbamate groups at the aluminum-coating interface, liberating amine functionality, which will increase the local pH due to their basic nature. These results also align with those of the solution model study.

CONCLUSIONS

It has been shown that amine containing monomers baring a *tert*-butylcarbamate functionality are able to be co-polymerized with epoxy-functional monomer GMA and formulated into a thermoset powder coating. The introduction of the BOC-Gly-MA monomer was shown to improve a coating's anti-corrosion performance (5-BOC-LT*), presenting the lowest average FFC track length, total FFC number (count), and total CSA, vs other experimental coatings in this study. Solution and coating models were designed to study the effect of filiform corrosion on the *tert*-butylcarbamate functional polymer, and specifically at the coating-aluminum interface. The study provided evidence to support the hypothesis that the *tert*-butylcarbamate protecting group can be removed from the polymer coating surface under the low pH (acidic) conditions of filiform corrosion, with the liberation of a basic primary amine, proposed to be the source for the material's improved anticorrosion performance.

It was shown that when polymerisation conditions are not optimized (HT), polymer advancement can occur through the formation of polymer-to-polymer bond forming reactions, inhibiting the polymer's ability to form a cohesive coating. The presence of advancement was then shown to be detrimental to a coating's material strength which resulted in a decrease in corrosion performance, with analysis finding an increase in a coating's Young's modulus (increase in coating stiffness) resulted in an increase in total CSA linked to increasing FFC width.

SUPPORTING INFORMATION

Spectral data and extended methodologies for synthesis, application and testing processes are supplied as Supporting Information

ACKNOWLEDGMENT

The authors would like to thank AkzoNobel and Northumbria University for financial support of this work and AkzoNobel for permission to publish this paper.

Author Contributions

The manuscript was written through contributions of all authors. All authors have given approval to the final version of the manuscript. All authors contributed equally.

REFERENCES

1. Olajire, A. A. Recent Advances on Organic Coating System Technologies for Corrosion Protection of Offshore Metallic Structures. *J. Mol. Liq*. **2018**, *269*, 572–606.

2. Banerjee, D., Guo, X., Benavides, J., Rameau, B. & Cloutier, S. G. Designing Green Self-healing Anticorrosion Conductive Smart Coating for Metal Protection. *Smart. Mater. Struct.* **2020**, *29*, 105027.

3. Du, Z. et al. The Review of Powder Coatings. *J. Mater. Sci. Chem. Eng.* **2016**, *04*, 54–59.

4. Prasad, L. K., McGinity, J. W. & Williams, R. O. Electrostatic Powder Coating: Principles and Pharmaceutical Applications. *Int. J. Pharm.* **2016**, *505*, 289–302.

5. Misev, T. A. & van der Linde, R. Powder Coatings Technology: New Developments at the Turn of the Century. *Prog. Org. Coat*. **1998**, *34*, 160–168.

6. Wei, H., Xia, J., Zhou, W., Zhou, L., Hussain, G., Li, Q., Ostrikov, Adhesion and Cohesion of Epoxy-based Industrial Composite Coatings. *Compos. B Eng*. **2020**, *193*, 108035.

7. Momber, A. W., Irmer, M. & Marquardt, T. Effects of Polymer Hardness on the Abrasive Wear Resistance of Thick Organic Offshore Coatings. *Prog. Org. Coat.* **2020**, *146*, 105720.

8. Fleetham, V., Gray E., Unthank, M. G., Acrylate Resins and Powder Coating Compositions and Powder Coated Substrates Including the Same, WO 2022/144219, **2022**.

9. Rossi, S., Powder and High-Solid Coatings. *Coatings* **2022**, *12*, 786.

10. Pélissier, K., Thierry, D., Powder and High-Solid Coatings as Anticorrosive Solutions for Marine and Offshore Applications: A Review. *Coatings* **2020**, *10*, 916.

11. Farshchi, N., Gedan-Smolka, M., Polyurethane Powder Coatings: A Review of Composition and Characterization. *Ind. Eng. Chem. Res*. **2020**, *59*, 15121–15132.

12. Yang, G., Xie, W., Huang, M., Champagne, V. K., Lee, J-H., Klier, J., Schiffman, J. D., Polymer Particles with a Low Glass Transition Temperature Containing Thermoset Resin Enable Powder Coatings at Room Temperature. *Ind. Eng. Chem. Res*. **2019**, *58*, 908–916.

13. Cambon, J. B,. Esteban, J., Ansart, F., Bonino, J. P., Turq, V., Santagneli, S. H., Santilli, C. V., Pulcinelli, S. H., Effect of Cerium on Structure Modifications of a Hybrid Sol–gel Coating, its Mechanical Properties and Anti-corrosion Behavior. *Mater. Res. Bull*. **2012**, *47*, 3170–3176.

14. Slabaugh, W. H. & Grotheer, M. Mechanism of Filiform Corrosion. *Ind. Eng. Chem*. **1954**, *46*, 1014–1016.

15. Halseid, M., Gundersen, J. T. B., Bauger, Ø., Hentschel, T. The Effect of Trace Additions of Copper and Pretreatment Conditions on the Filiform Corrosion of Powder-Coated Aluminium Alloy AA6060. *Surf. Interface Anal.* **2019**, *51* (12), 1225–1230.

16. Nardeli, J. V., Snihirova, D. V, Fugivara, C. S., Montemor, M. F., Pinto, E. R. P., Messaddecq, Y., Benedetti, A. V. Localised Corrosion Assessment of Crambe-Oil-Based Polyurethane Coatings Applied on the ASTM 1200 Aluminium Alloy. *Corros. Sci.* **2016**, *111*, 422–435.

17. a) Kakaroglou, A., Nisol, B., Hauffman, T., De Graeve, I., Reniers, F., Van Assche, G., Terryn, H. Incorporation of Corrosion Inhibitor in Plasma Polymerized Allyl Methacrylate Coatings and Evaluation of Its Corrosion Performance. *Surf. Coat. Technol.* **2014**, *259*, 714–724. b) Wonnie Ma, I. A., Ammar, Sh., Sachin S. A., Ramesh, K. K., Ramesh, S., A Concise Review on Corrosion Inhibitors: Types, Mechanism and Electrochemical Evaluation Studies. *J. Coat. Technol. Res*., **2022**, *19* (1), 241–268.

18. Jegdić, B., Bobić, B., Linić, S. Corrosion Behaviour of AA2024 Aluminium Alloy in Different Tempers in NaCl Solution and with the $CeCl_3$ Corrosion Inhibitor. *Mater. and Corros.* **2020**, *71* (3), 352–364.

19. Pirhady Tavandashti, N., Ghorbani, M., Shojaei, A., Mol, J. M. C., Terryn, H., Baert, K., Gonzalez-Garcia, Y. Inhibitor-Loaded Conducting Polymer Capsules for Active Corrosion Protection of Coating Defects. *Corros. Sci.* **2016**, *112*, 138–149.

20. Chawada, G., Dholakiya, B. Z. Influence of Organic Corrosion Inhibitors on the Corrosion Performance of Organic–Inorganic Hybrid Coatings Applied on Aluminium Alloy. *Res. Chem Intermed.* **2016**, *42* (2), 545–557.

21. Xhanari, K., Finšgar, M. Organic Corrosion Inhibitors for Aluminium and Its Alloys in Acid Solutions: A Review. *RSC Adv.* **2016**, *6* (67), 62833–62857.

22. Bautista, A. Filiform Corrosion in Polymer-Coated Metals. *Prog. Org. Coat.* **1996**, *28* (1), 49–58.

23. Delplancke, J. L., Berger, S., Lefèbvre, X., Maetens, D., Pourbaix, A., Heymans, N. Filiform Corrosion: Interactions Between Electrochemistry and Mechanical Properties of the Paints. *Prog. Org. Coat.* **2001**, *43* (1–3), 64–74.

24. Visser, P., Terryn, H., Mol, J. M. C. On the Importance of Irreversibility of Corrosion Inhibitors for Active Coating Protection of AA2024-T3. *Corros. Sci.* **2018**, *140*, 272–285.

25. Visser, P., Terryn, H., Mol, J. M. C. Active Corrosion Protection of Various Aluminium Alloys by Lithium-leaching Coatings. *Surf. Interface Anal.* **2019**, *51* (12), 1276–1287.

26. Visser, P., Lutz, A., Mol, J. M. C., Terryn, H. Study of the Formation of a Protective Layer in a Defect from Lithium-Leaching Organic Coatings. *Prog. Org. Coat.* **2016**, *99*, 80–90.

27. Visser, P., Liu, Y., Terryn, H., Mol, J. M. C. Lithium Salts as Leachable Corrosion Inhibitors and Potential Replacement for Hexavalent Chromium in Organic Coatings for the Protection of Aluminium Alloys. *J. Coat. Technol. Res.* **2016**, *13* (4), 557–566.

28. Li, Z., Homborg, A., Gonzalez-Garcia, Y., Kosari, A., Visser, P., Mol, A. Evaluation of the Formation and Protectiveness of a Lithium-Based Conversion Layer Using Electrochemical Noise. *Electrochim. Acta.* **2022**, *426*, 140733.

29. Marcoen, K., Visser, P., Trindade, G. F., Abel, M.-L., Watts, J. F., Mol, J. M. C., Terryn, H., Hauffman, T. Compositional Study of a Corrosion Protective Layer Formed by Leachable Lithium Salts in a Coating Defect on AA2024-T3 Aluminium Alloys. *Prog. Org. Coat.* **2018**, *119*, 65–75.

30. Visser, P., Liu, Y., Zhou, X., Hashimoto, T., Thompson, G. E., Lyon, S. B., van der Ven, L. G. J., Mol, A. J. M. C., Terryn, Herman. A. The Corrosion Protection of AA2024-T3 Aluminium Alloy by Leaching of Lithium-Containing Salts from Organic Coatings. *Faraday Discuss.* **2015**, *180*, 511–526.

31. Pachayappan, L., Kamath, P. V. Reversible Hydration of the Perchlorate-Intercalated Layered Double Hydroxides of Li and Al: Structure Models for the Dehydrated Phases. *Bull. Mater. Sci.* **2020**, *43* (1), 141.

32. Liu, Y., Visser, P., Zhou, X., Lyon, S. B., Hashimoto, T., Curioni, M., Gholinia, A., Thompson, G. E., Smyth, G., Gibbon, S. R., Graham, D., Mol, J. M. C., Terryn, H. Protective Film Formation on AA2024-T3 Aluminum Alloy by Leaching of Lithium Carbonate from an Organic Coating. *J. Electrochem. Soc.* **2016**, *163* (3), 45–53.

33. Unthank, M. G., Cameron, C., Wright, A., Hughes, D., Alam, M. A., Probert, M. R. Amino-Diol Borate Complexation for Controlling Transport Phenomena of Penetrant Molecules into Polymeric Matrices. *Polym. Chem.* **2019**, *10* (36), 4920–4929.

34. Anderson, L., Sanders, E. W., Unthank, M. G. Recyclable Thermosets Based on Modified Epoxy-Amine Network Polymers. *Mater. Horiz.* **2023**, *10*, 889-898.

35. Morsch, S., Liu, Y., Lyon, S. B., Gibbon, S. R., Gabriele, B., Malanin, M., Eichhorn, K.-J. Examining the Early Stages of Thermal Oxidative Degradation in Epoxy-Amine Resins. *Polym. Degrad. Stab.* **2020**, *176*, 109147.

36. Bourne-Branchu, Y., Gosmini, C., Danoun, G. N -Boc-Amides in Cross-Coupling Reactions. *Chem. - Eur. J.* **2019**, *25* (11), 2663–2674.

37. Singh, A., Maikhuri, V. K., Verma, V., Chhatwal, R. J., Prasad, A. K. Synthesis and Carboxylate Anion Binding Studies on Cyclic Sugar-Amino Acid Hybrids. *Synth. Commun.* **2020**, *50* (18), 2787–2795.

38. Axundova, F. N., Kurbanova, M. M., Huseynzada, A. E., Alves, M. J. Synthesis of New Iminosugar Derivatives. *Russ. J. Org. Chem*. **2019**, *55* (12), 1975–1978.

39. Jing, C., Suzuki, Y., Matsumoto, A. Thermal Decomposition of Methacrylate Polymers Containing *tert* -Butoxycarbonyl Moiety. *Polym. Degrad. Stab.* **2019**, *166*, 145–154.

40. Veloso, S. R. S., Jervis, P. J., Silva, J. F. G., Hilliou, L., Moura, C., Pereira, D. M., Coutinho, P. J. G., Martins, J. A., Castanheira, E. M. S., Ferreira, P. M. T. Supramolecular Ultra-Short Carboxybenzyl-Protected Dehydropeptide-Based Hydrogels for Drug Delivery. *Mater. Sci. Eng. C.* **2021**, *122*, 111869.

41. Murphy, R. D., Bobbi, E., Oliveira, F. C. S., Cryan, S., Heise, A. Gelating Polypeptide Matrices Based on the Difunctional *N* -carboxyanhydride Diaminopimelic Acid Cross-linker. *J. Polym. Sci. A Polym. Chem.* **2019**, *57* (11), 1209–1215.

42. Jones, J. a-Amino protection. *Amino Acid and Peptide Synthesis*, 2nd ed., Oxford University Press: USA, **2002**., 7, 17-19.

43. Aladini, F., Araman, C., Becker, C. F. W. Chemical Synthesis and Characterization of Elastin-like Polypeptides (ELPs) with Variable Guest Residues. *J. Pept. Sci.* **2016**, *22* (5), 334–342.

44. Donovan, A. J., Dowle, J., Yang, Y., Weiss, M. A., Kent, S. B. H. Total Synthesis of Bovine Pancreatic Trypsin Inhibitor and the Protein Diastereomer [Gly37D-Ala]BPTI Using Boc Chemistry Solid Phase Peptide Synthesis. *Pept, Sci.* **2020**, 4, *112*.

45. Muttenthaler, M., Albericio, F., Dawson, P. E. Methods, Setup and Safe Handling for Anhydrous Hydrogen Fluoride Cleavage in Boc Solid-Phase Peptide Synthesis. *Nat. Protoc.* **2015**, *10* (7), 1067–1083.

46. Jain, A. K., Gupta, V. K., Bhatnagar, A., Suhas. Utilization of Industrial Waste Products as Adsorbents for the Removal of Dyes. *J. Hazard. Mater.* **2003**, *101* (1), 31–42.

47. Ghosh, S., Setia, S., Sidiq, S., Pal, S. K. A New Visual Test for P-Quinone and Its Relevance to the Biodiesel Industry. *Anal. Methods.* **2012**, *4* (11), 3542-3544.

48. Ullah, S. Evaluation of Steric Effect of Hydroquinone, Tert-Butyl Hydroquinone and 2, 5-Ditert-Butyl Hydroquinone by Using a Briggs-Rauscher Oscillator. *Int. J. Electrochem. Sci.* **2018**, 11819–11828.

49. Li, Y., Wu, X., Wu, Z., Zhong, M., Su, X., Ye, Y., Liu, Y., Tan, L., Liang, Y. Colorimetric Sensor Array Based on CoOOH Nanoflakes for Rapid Discrimination of Antioxidants in Food. *Anal. Methods.* **2022**, *14* (28), 2754–2760.

50. Wu, Y., Fei, M., Qiu, R., Liu, W., Qiu, J. A Review on Styrene Substitutes in Thermosets and Their Composites. *Polymers*, **2019**, *11*(11), 1815.

51. Flory, P. J. Molecular Size Distribution in Three Dimensional Polymers. I. Gelation. *J. Am. Chem. Soc.,* **1941**, *63*(11), 3083-3090.

52. a) Stockmayer, W. H. Theory of Molecular Size Distribution and Gel Formation in Branched Polymers II. General Cross Linking. *J. Chem. Phys.*, **1944**, *12*(4), 125-131.54. b) Odian, G., Statistical Approach to Gelation. *Principles of Polymerization*, 4th ed., John Wiley and Sons inc, USA, **2004**. 108-110.

53. Vidil, T., Tournilhac, F., Musso, S., Robisson, A., Leibler, L. Control of Reactions and Network Structures of Epoxy Thermosets. *Prog. Polym. Sci.* **2016**, *62*, 126–179.

54. Brocas, A.-L., Mantzaridis, C., Tunc, D., Carlotti, S. Polyether Synthesis: From Activated or Metal-Free Anionic Ring-Opening Polymerization of Epoxides to Functionalization. *Prog. Polym. Sci.* **2013**, *38* (6), 845–873.

55. Su, S., Wang, H., Zhou, C., Wang, Y., Liu, J. Study on Epoxy Resin with High Elongation-at-Break Using Polyamide and Polyether Amine as a Two-Component Curing Agent. *e-Polymers.* **2018**, *18* (5), 433–439.

56. Savonnet, E., le Coz, C., Grau, E., Grelier, S., Defoort, B., Cramail, H. Divanillin-Based Aromatic Amines: Synthesis and Use as Curing Agents for Fully Vanillin-Based Epoxy Thermosets. *Front. Chem.* **2019**, *7*, 606.

57. Bassampour, Z. S., Budy, S. M., Son, D. Y. Degradable Epoxy Resins Based on Bisphenol A Diglycidyl Ether and Silyl Ether Amine Curing Agents. *J. Appl. Polym. Sci.* **2017**, *134* (12), 44620–44628.

58. P. A. L. Robert J. Young, An Introduction to Polymers, 3rd., CRC Press, **2011**. 391–396.

59. I. M. Kalogeras, An Encyclopedia of Polymer Blends, Wiley, **2016**. 37–38.

60. Watson, T. M., Coleman, A. J., Williams, G., McMurray, H. N. The Effect of Oxygen Partial Pressure on the Filiform Corrosion of Organic Coated Iron. *Corros. Sci.* **2014**, *89* (C), 46–58.